Effect of Tensile Strain on Performance Parameters of Different Structures of MoS_2 Monolayer

Priya kaushal (pkaushal2407@gmail.com)
NIT Hamirpur: National Institute of Technology Hamirpur
Tarun Chaudhary
NIT Jalandhar: Dr BR Ambedkar National Institute of Technology
Gargi Khanna
NIT Hamirpur: National Institute of Technology Hamirpur

Research Article

Keywords: Two-dimensional materials, MoS2 monolayer, First principles, Strain effect

Posted Date: June 1st, 2021

DOI: https://doi.org/10.21203/rs.3.rs-503274/v1

Version of Record: A version of this preprint was published at Silicon on July 26th, 2021. See the published version at https://doi.org/10.1007/s12633-021-01256-4.

Abstract

The present work is based on the computational study of MoS_2 monolayer and effect of tensile strain on its atomic level structure. The bandgap for MoS_2 monolayer, defected MoS_2 monolayer and Silicon-doped monolayer are 1.82 eV (direct bandgap), 0.04 (indirect bandgap) and 1.25eV (indirect bandgap), respectively. The impact of tensile strain (0-0.7%) on the bandgap and effective mass of charge carriers of these three MoS_2 structure has been investigated. The bandgap decrease of 5.76%, 31.86% and 6.03% has been observed in the three structures for biaxial strain while the impact of uniaxial strain is quite low. The impact of higher temperature on the bandgap under biaxial tensile strain has been also analyzed in this paper. These observations are extremely important for 2D material-based research for electronic applications.

1 Introduction

The nanotechnology has allowed the researchers to work up to a nanoscale and offered extraordinary results which were never possible earlier. The nanotechnologies include highly sensitive sensors, high-performance nanoelectronics, nanocomposites, and innovative medicines and cancer therapy based on nanoparticles [1-4]. The development of nanotechnology has also proposed the different classes of dimensional systems which are zero-dimensional (0D, e.g., nanoparticles), one-dimensional (1D, e.g., nanowires), two-dimensional (2D, e.g., graphene), and three-dimensional (3D, e.g., bulk materials). The low dimensional systems play major role to differentiate the nanomaterials, as they explore the atomic structure of materials and properties of the low dimensional materials [5].

In 2004, the experimental discovery of graphene is one of the most important scientific revolution of the 20^{th} century [6]. The two-dimensional (2D) crystal of graphene is created by separating it from graphite material [7-9]. Graphene is a single layer structure of carbon atoms arranged in the honeycomb form. Graphene material has the potential for high-speed nanoelectronics applications because of its unique

features like extremely high carrier mobility and half-integer quantum effects. Because of high mechanical and chemical stability, we can use it in different working conditions [10,11]. Looking into the potential of 2D materials, graphene-like inorganic monolayer materials gallium nitride (GaN) [12], silicon carbide (SiC) [13,14], boron nitride (BN) [15], zinc oxide (ZnO) [16,17], aluminum nitride (AlN) [18-20] and transition-metal dichalcogenides (TMDs) [21,22] have been synthesized and analyzed for various parameters. Among these 2D materials, the TMDs have shown a broad range of mechanical, electronics, optical, thermal, and chemical properties [23,24]. The monolayer of TMDs (such as MX_2 where M=Mo, W; and X=S, Se, Te, etc.) having a honeycomb structure where transition metal atoms (M) are switched between chalcogen atoms X. All the atoms in a monolayer of TMD are attached by the covalent force and the different layers are attached by van der Waals forces. For electronics applications, the TMDs like MoS_2, $MoSe_2$, $MoTe_2$, WS_2, and WSe_2 have shown extraordinary features. In bulk form, TMDs are indirect bandgap semiconductors. By thinning down to a single layer, the indirect bandgap changes into a direct bandgap. The monolayer direct bandgap of TMD is in the range of (1.1-2.0eV) at the K-point in the Brillion

zone [25-27]. In this work, we have focused on bandgap and effective mass of MoS_2 monolayer for without strain and with strain structure. We also investigated the same for defected monolayer and silicon-doped (Si-doped) monolayer.

1.1 Related Work

S. Deng et al., [28] have investigated the response of 2D TMDs on a mechanical strain by using first-principles methods. By studying the mechanical properties of 2D TMDs it has been found that the stable range of strain is determined by the young's modulus. Moreover, it has been also analyzed that the strain also induces the electronic bandgap properties. X Wang e al., [29] have presented a theoretical study report for the interaction of No_2 molecule with the Mo-edge of MoS_2 zigzag nanoribbon, and for its simulations, the density functional theory (DFT) method has been used. The effect of uniaxial tensile strain on the physical and structural properties of MoS_2 Nanoribbon and the absorption process has been discussed in detail. It has been observed that there is increase in the magnitude of the adsorption energy and a more stable structure is obtained with strain. S. Yua et al., [30] have presented the computational study of MoS_2 monolayer under tensile strain. The transition from direct to indirect and semiconductor to metal has been investigated under the tensile strain along with both x-direction and y-direction. The phase transition, carrier mobility, and effective mass of MoS_2 monolayer have been studied under tensile strain. The mobility increases when the biaxial strain $\varepsilon_x=\varepsilon_y=9.5\%$ has been applied. Additionally, the mobility parameter with an increase in temperature has been decreased monotonically. J. Ni et al., [31] have demonstrated the modulation of bandgap transition of two heterostructures i.e. Blue P/GeC and Blue P/SiC with strain engineering. According to the authors, the electronic structure and optical properties of the Blue P/GeC and Blue P/SiC have changed under strain. R. Beiranvand [32] has investigated the electrical and optical properties of TMDs MoX_2 (X = S, Se, Te) based on the DFT method. Also, the author has studied the optical absorption coefficient, real and imaginary parts of the dielectric functions, reflectivity, and energy loss functions for external electric fields along with two directions in detail. The high absorption coefficient value is the remarked property of the MoX_2 monolayer which makes these materials best for optoelectronics applications. A. O. M. Almayyali et al., [33] have investigated the optical and electronics of zinc iodide (ZnI_2) material under the impact of the biaxial strain. For the ZnI_2 material-based calculation of molecular dynamic simulations, binding energy, and phonon dispersion curve it has been observed that the ZnI_2 has high stability. According to the results it has been observed that the ZnI_2 monolayer behave as a semiconductor having an indirect bandgap under PBF and HSE06 methods and values of bandgaps are 2.018eV and 2.94eV, respectively. M. Y. Liu et al. [34] have proposed a new class of 2D materials XBi (where X=Si, Ge, Sn, and Pb) along with the metal monochalogenide structure to provide tunable orbital properties. It has been found that the spin-orbit coupling shifts the SnBi electronics properties from semiconductor to metal, and the applied strain can lead toward a novel Dirac electronic state. Surface chemical decoration has been confirmed to be an effective path to achieve the Bi-pz filtering effect and p-p inversion in the orbital. Y. Solyaev et al., [35] have investigated the electric field, inertia gradient, and strain impact on anti-plane wave propagation of piezoelectric materials. It has been analyzed that the model represents a normal dispersion of short wave

in piezoelectric materials. Another model parameter on the phase velocity, attenuation of shear horizontal, and coupled electromechanical factor have been investigated. It has been concluded that the results obtained in this article can be applied for the analysis of small-scale piezoelectric structures and high-frequency MEMS/NEMS. H. Li et al., [36] have explored a novel 2D bonding heterostructure that consists of a hexagonal borophene monolayer attached with two blue phosphorene layers. The proposed heterostructure having good conductivity, high stability, and high in-plane stiffness. Later, the proposed novel 2D heterostructure has been investigated by using the DFT method as an acceptable material for lithium-sulfur batteries. The results have shown that the lithium-polysulfides based on the proposed structure having proper adsorption energies i.e., 0.60-2.68 eV, and moderate diffusion barrier i.e., 0.09-0.31 eV. D.M. Hoat et al., [37] have investigated the electronic structure and optical properties of Hafnium disulfide (HfS_2) under vertical strain using DFT calculations. By calculating the phonon dispersion curves the dynamical stability of the HfS_2 monolayer has been examined. The HfS_2 monolayer has shown a high absorption coefficient of 49.6000 (10^4 /cm) and 88.122 (10^4 /cm) in the visible and ultraviolet regions, respectively which display promising optoelectronic applicability.

2 Computational Details

For this study, we use the DFT method in Virtual Nanolab Atomistix ToolKit (ATK) [38] for first-principle calculation. In the basis setting of the ATK-DFT method, we use localized density approximation (LDA) exchange-correlation along with density mesh cut-off energy value of 75 Hartree and a double Zeta polarized (DZP) [39]. All the simulations with strain and without strain are done at room temperature. The unit cell selected for simulation containing two Mo and four S atoms with a periodic boundary. The Monkhorst-Pack k-grid mesh value for our simulation is 11x11x1. All the lattice constant, atomic positions, and atomic bonds are optimized by applying the limited-memory Broyden–Fletcher–Goldfarb–Shanno (L-BFGS) [40] which is a quasi-Newton- type minimization technique, and set the value for force and stress tolerance equal to 0.05 eV/Å. The Pulay-mixer algorithm with a 10^{-5} tolerance value is applied as iteration control in ATK-DFT. The 100 steps are set for maximum numbers of full self-consistent field (SCF) iteration. The Hamiltonian variable is used in the mixing variable. The Fast Fourier Transform (FFT) Poisson solver under ATK-DFT with a periodic boundary condition. The simple orthorhombic lattice constant and angles of TMDs are described in Table 1.

3 Simulation Results

At first, we discuss the structures of MoS_2 monolayer that going to investigated in this work. Fig. 1 show the atomistic lattice structure of MoS_2 monolayer, where the supercell geometry is orthorhombic and the small rectangular structure shown with solid line is used for elastic constant calculation. To study the carrier conduction in the armchair [1,0] and zigzag [0,1] directions, the orthorhombic geometry is created in supercell. The defected MoS_2 structure where one S atom is removed from structure and Si-doped MoS_2 monolayer where one S atom is replaced with one Silicon atom shown in fig. 2. First parameter that we discuss is band structure of different additions of MoS_2 monolayer. In band structure calculation we

set the 100 points per segment and Γ-Y-X-Γ Brillouin zone route. The K-points which is the fractional reciprocal coordinates in hexagonal lattice equal to (1/3,1/3), but in orthorhombic supercell [41] it is equivalent to (1/3,0) lies a midpoint between Γ and Y points. The band structure along with density of states (DoS) of unstrained atomic structures of MoS_2 monolayer is shown in fig. 3. The bandgap value for MoS_2 Monolayer, Defected MoS_2 Monolayer and Si-Doped MoS_2 monolayer are 1.820001eV (direct bandgap), 0.04417 eV (indirect bandgap) and 1.252501eV (indirect bandgap), respectively.

Table 1 Lattice parameters of TMDs monolayers

Material	a(Å)	b(Å)	Bond Length(Å)	α	β	γ	Bandgap (eV)
MoS_2	5.47397	3.1604	2.41763	90º	90º	90º	1.820001
$MoSe_2$	5.69498	3.288	2.53048	90º	90º	90º	1.581859
$MoTe_2$	6.0937	3.5182	2.71074	90º	90º	90º	1.17133
WS_2	5.4615	3.5132	2.40475	90º	90º	90º	1.887673
WSe_2	5.68459	3.282	2.52168	90º	90º	90º	1.623808

Next, we explore the electronics properties of three MoS_2 structures with tensile strain. The vector components of strain along x-direction [1,0] and y-direction [0,1] are denoted as ε_x and ε_y, respectively. This study calculated the tensile strain as the relative lattice stretching percentage, given by

$$\varepsilon_x = \frac{a-a_0}{a_0} \times 100 \text{ and } \varepsilon_y = \frac{b-b_0}{b_0} \times 100 \qquad (1)$$

Where, a_0 and b_0 are the lattice constant of unstrained structure. The a and b are the new lattice dimension due to tensile strain. In this work the uniaxial strain in the range of 0-0.7% of lattice constant with 0.1% step size along X and Y direction has been applied. Fig. 4 shows the results of uniaxial and biaxial strains on different structures. From figure 4(a), it is observed that the bandgap percentage decrease in monolayer MoS_2 is 1.99% for strain along both X and Y directions but in the case of biaxial direction the percentage decrease is 5.45%. For defected layer the percentage decrease in bandgap is 14.32%, 20.17% and 31.86% for the strain in X-direction, Y-direction and biaxial, respectively. For Si-doped monolayer the percentage decrease in bandgap for uniaxial strain in X-direction, Y-direction and biaxial are 4.69%, 1.36% and 6.03%.

When the strain applied to a structure, it also effects the energy band curvature which is proportional to the carrier effective mass(m):

$$m^* = \frac{\hbar^2}{\partial^2 E/\partial k^2} \qquad (2)$$

Where, $\hbar$ = Planck Constant, E = Energy and k = Momentum.

For monolayer we investigate the electron effective mass (m_e*) at fractional K-points (0,0.335,0), hole effective mass(m_h*) at fractional K-points (0,0.335,0) and Γ (0,0,0) under tensile strain. The same effective mass calculation done for defected monolayer and Si-doped monolayer. Table 2 shows the values of carrier effective mass of different structures of MoS_2 monolayer without strain. Fig. 5 shows the hole and electron effective mass at different tensile value from 0-0.7%. As shown in fig. 5 the effective mass value under tensile strain change with different rate along the three directions.

Table 2 Effective mass of different MoS_2 structures without strain

Structures	m_e* at K-points	m_h* at K-points	m_h* at Γ-points
MoS_2 Monolayer	0.475	0.602	2.65
Defected MoS_2 Monolayer	0.301	0.209	0.139
Si-doped MoS_2 Monolayer	0.492	0.743	1.987

We have also analyzed the effect of increase in temperature on the bandgap. Fig. 6 shows the change in bandgap with respect to biaxial tensile strain under various temperature conditions. In the case of defected monolayer for temperature 25ºC and 50ºC the bandgap is almost same under the strain, depicted by the almost overlaping lines in fig. 6(b). The bandgap percentage decrease for various temperature is calculated and listed in Table 3.

Table 3 Bandgap Decreasing rate at different higher temperature.

Structure	25˚C	50ºC	100ºC
MoS_2 Monolayer	5.49%	5.55%	5.55%
Defected MoS_2 Monolayer	31.81%	33.63%	36.58%
Silicon Doped MoS_2 Monolayer	6.4%	6.77%	8.31%

Conclusion

In summary, we have investigated the different MoS_2 monolayers such as simple monolayer, defect of S atom in monolayer, and Silicon doped monolayer using first principle calculation method. After that, we

have studied these structures under the tensile strain of range 0-0.7% with steps size of 0.1%. For the analysis purpose, we explore the two electronics properties i.e., band structure and effective mass for holes and electrons. It is observed that the bandgap is decreased harmoniously and monotonically with the rise of strain. The strain in [1,0], [0,1] and [1,1] directions have same role for bandgap modulation. However, the observed effective mass values are behaving differently for tensile strain along [1,0], [0,1], and [1,1] directions. The bandgap modulation analysis at higher temperature also has been done. In conclusion, the computational study achieved in this work can help the research on further applications of 2D materials and devices.

Declarations

Funding:

The authors are thankful to National Institute of Technology Hamirpur (HP) for supporting this research work. However, no funding was received with the preparation of this manuscript.

Conflicts of Interest/Competing interest:

Authors have no conflict of interest.

Availability of Data and Material:

All data and materials comply with field standards.

Code availability: We have used VNL-ATK QuantumWise Software for implementation.

Author's Contributions:

All authors contributed to the study conception, simulation and analysis. All the authors have contributed in writing the manuscript and approved the final manuscript.

Ethics approval

The reported work did not involve any human's participation and/or did not harm welfare of animals.

Consent to Participate:

Not required as this manuscript does not contain participation of humans/children/animals.

Consent for publication:

Not required as this manuscript does not contain participation of humans/children/animals.

References

1. Davis ME, Zuckerman JE, Choi, CHJ, Seligson D, Tolcher A, Alabi CA, Yen Y, Heidel J, & Ribas A (2010) Evidence of RNAi in humans from systemically administered siRNA via targeted nanoparticles. Nature 464:1067-1070. https://doi.org/10.1038/nature08956
2. Joseph JD, Kumaragurubaran B, & Sathish S (2019) Effect of MoS_2 on the Wear Behavior of Aluminium (AlMg0. 5Si) Composite. Silicon 12:1-9. https://doi.org/10.1007/s12633-019-00238-x
3. Karakoti AS, Tsigkou O, Yue S, Lee PD, Stevens MM, Jones JR, & Seal S (2010) Rare earth oxides as nanoadditives in 3-D nanocomposite scaffolds for bone regeneration. Journal of Materials Chemistry 20:8912-8919. https://doi.org/10.1039/C0JM01072C
4. Tiwari JN, Tiwari RN, & Kim KS (2012) Zero-dimensional, one-dimensional, two-dimensional and three-dimensional nanostructured materials for advanced electrochemical energy devices. Progress in Materials Science 57:724-803. https://doi.org/10.1016/j.pmatsci.2011.08.003
5. Mas-Balleste R, Gomez-Navarro C, Gomez-Herrero J, & Zamora F (2011) 2D materials: to graphene and beyond. Nanoscale 3:20-30. https://doi.org/10.1039/C0NR00323A
6. Boochani A, & Veisi S (2018) The Vanadium Effect on Electronic and Optical Response of MoS_2 Graphene-Like: Using DFT. Silicon 10:2855-2863. https://doi.org/10.1007/s12633-018-9825-0
7. Novoselov KS, Jiang D, Schedin F, Booth TJ, Khotkevich VV, Morozov SV, & Geim AK (2005) Two-dimensional atomic crystals. Proceedings of the National Academy of Sciences 102:10451-10453. https://doi.org/10.1073/pnas.0502848102
8. Novoselov KS, Geim AK, Morozov SV, Jiang D, Katsnelson MI, Grigorieva IV, Dubonos SV & Firsov AA (2005) Two-dimensional gas of massless Dirac fermions in graphene. nature, 438:197-200. https://doi.org/10.1038/nature04233
9. Geim AK & Novoselov KS (2010) The rise of graphene.: a review. Nanoscience and technology 11-19. https://doi.org/10.1142/9789814287005_0002
10. Choi W, Lahiri I, Seelaboyina R, & Kang YS (2010) Synthesis of graphene and its applications: a review. Solid State and Materials Sciences 35:52-71. https://doi.org/10.1080/10408430903505036
11. Allen MJ, Tung VC, & Kaner RB (2010) Honeycomb carbon: a review of graphene. Chemical reviews 110:132-145. https://doi.org/10.1021/cr900070d
12. Beiranvand R, & Valedbagi S (2016) Electronic and optical properties of advance semiconductor materials: BN, AlN and GaN nanosheets from first principles. Optik,127:1553-1560. https://doi.org/10.1016/j.ijleo.2015.10.194
13. Shi Z, Zhang Z, Kutana A, & Yakobson BI (2015) Predicting two-dimensional silicon carbide monolayers. ACS nano 9:9802-9809. https://doi.org/10.1021/acsnano.5b02753
14. Javan MB (2016) Electronic and magnetic properties of monolayer SiC sheet doped with 3d-transition metals. Journal of Magnetism and Magnetic Materials 401:656-661. https://doi.org/10.1016/j.jmmm.2015.10.103
15. Beiranvand R & Valedbagi S (2015) Electronic and optical properties of h-BN nanosheet: A first principles calculation. Diamond and Related Materials 58:190-

195. https://doi.org/10.1016/j.diamond.2015.07.008

16. Chaurasiya R, Dixit A, & Pandey R (2019) Strain-driven thermodynamic stability and electronic transitions in ZnX (X= O, S, Se, and Te) monolayers. Journal of Applied Physics 125: 082540. https://doi.org/10.1063/1.5053680
17. Pradhan D, & Kar JP (2021) Role of Process Parameters on Microstructural and Electronic Properties of Rapid Thermally Grown MoS_2 Thin Films on Silicon Substrates. Silicon 1-11. https://doi.org/10.1007/s12633-021-00959-y
18. Aghili S, Beiranvand R, Elahi SM, & Abolhasani MR (2016) Half-metallic ferromagnetism in Mn-doped zigzag AlN nanoribbon from first-principles. Journal of Magnetism and Magnetic Materials 420:122-128. https://doi.org/10.1016/j.jmmm.2016.06.067
19. Beiranvand R (2016) Electronic and magnetic properties of Cd-doped zigzag AlN nanoribbons from first principles. Rare Metals 35:771-778. https://doi.org/10.1007/s12598-015-0471-z
20. Chegeni M, Beiranvand R & Valedbagi S (2017) Generating Tunable Magnetism in AlN Nanoribbons Using Anion/Cation Vacancies: a First-Principles Prediction. Brazilian Journal of Physics 47:137-144. https://doi.org/10.1007/s13538-016-0480-x
21. Papageorgiou DG, Kinloch IA, & Young RJ (2017) Mechanical properties of graphene and graphene-based nanocomposites. Progress in Materials Science 90:75-127. https://doi.org/10.1016/j.pmatsci.2017.07.004
22. Peres NM, Araújo MA, & Bozi D (2004) Phase diagram and magnetic collective excitations of the Hubbard model for graphene sheets and layers. Physical Review B 70:195122. https://doi.org/10.1103/PhysRevB.70.195122
23. Wang QH, Kalantar-Zadeh K, Kis A, Coleman J N, & Strano MS (2012) Electronics and optoelectronics of two-dimensional transition metal dichalcogenides. Nature nanotechnology 7:699-712. https://doi.org/10.1038/nnano.2012.193
24. Chhowalla M, Liu Z, & Zhang H (2015) Two-dimensional transition metal dichalcogenide (TMD) nanosheets. Chemical Society Reviews 44:2584-2586. https://doi.org/10.1039/C5CS90037A
25. Mak KF, Lee C, Hone J, Shan J, & Heinz TF (2010) Atomically thin MoS_2: a new direct-gap semiconductor. Physical review letters 105:136805. https://doi.org/10.1103/PhysRevLett.105.136805
26. Gutierrez HR, Perea-Lopez N, Elías AL, Berkdemir A, Wang B, Lv R, Lopez-Urias F, Crespi VH, Terrones H & Terrones M (2013) Extraordinary room-temperature photoluminescence in triangular WS_2 Nano letters 13:3447-3454. https://doi.org/10.1021/nl3026357
27. Chang CH, Fan X, Lin SH, & Kuo JL (2013) Orbital analysis of electronic structure and phonon dispersion in MoS_2, $MoSe_2$, WS_2, and WSe_2 monolayers under strain. Physical Review B 88:195420. https://doi.org/10.1103/PhysRevB.88.195420
28. Deng S, Li L, & Li M (2018) Stability of direct band gap under mechanical strains for monolayer MoS_2, $MoSe_2$, WS_2 and WSe_2. Physica E: Low-dimensional Systems and Nanostructures 101:44-49.

https://doi.org/10.1016/j.physe.2018.03.016

29. Wang X, & Shi J (2017) Strain effects on the interaction between NO_2 and the Mo-edge of the MoS2 zigzag nanoribbon. IEEE Transactions on Nanotechnology 16:982-990. https://doi.org/10.1109/TNANO.2017.2737942
30. Yu S, Xiong HD, Eshun K, Yuan H, & Li Q (2015) Phase transition, effective mass and carrier mobility of MoS_2 monolayer under tensile strain. Applied Surface Science 325:27-32. https://doi.org/10.1016/j.apsusc.2014.11.079
31. Ni J, Quintana M, Jia F, & Song S (2021) Tailoring the electronic and optical properties of layered blue phosphorene/XC (X= Ge, Si) vdW heterostructures by strain engineering. Physica E: Low-dimensional Systems and Nanostructures 127:114460. https://doi.org/10.1016/j.physe.2020.114460
32. Beiranvand R (2021) Theoretical investigation of electronic and optical properties of 2D transition metal dichalcogenides MoX_2 (X= S, Se, Te) from first-principles. Physica E: Low-dimensional Systems and Nanostructures 126:114416. https://doi.org/10.1016/j.physe.2020.114416
33. Almayyali AO, Muhsen HO, Merdan M, Obeid MM, & Jappor HR (2021) Two-dimensional ZnI_2 monolayer as a photocatalyst for water splitting and improvement its electronic and optical properties by strains. Physica E: Low-dimensional Systems and Nanostructures 126:114487. https://doi.org/10.1016/j.physe.2020.114487
34. Liu MY, Gong L, Li WZ, Zhang ML, He Y, & Cao C (2021) Band engineering of XBi (X= Si, Ge, Sn, and Pb) single layers via strain and surface chemical-modulation. Applied Surface Science 540:148268. https://doi.org/10.1016/j.apsusc.2020.148268
35. Solyaev Y, & Lurie S (2021) Electric field, strain and inertia gradient effects on anti-plane wave propagation in piezoelectric materials. Journal of Sound and Vibration 494:115898. https://doi.org/10.1016/j.jsv.2020.115898
36. Li H, Hou J, Duan Q, & Jiang D (2021) Hexagonal borophene sandwiched between blue phosphorenes: A novel bonding heterostructure as an anchoring material for lithium-sulfur batteries. Applied Surface Science 545:148770. https://doi.org/10.1016/j.apsusc.2020.148770
37. Hoat DM, Ponce-Perez R, Vu TV, Rivas-Silva JF, & Cocoletzi GH (2021) Theoretical analysis of the HfS_2 monolayer electronic structure and optical properties under vertical strain effects. Optik 225:165718. https://doi.org/10.1016/j.ijleo.2020.165718
38. Atomistix ToolKit (ATK), https://quantumwise.com/
39. Kohn W, & Sham LJ (1965) Self-consistent equations including exchange and correlation effects. Physical review 140:A1133. https://doi.org/10.1103/PhysRev.140.A1133
40. Liu DC & Nocedal J (1989) On the limited memory BFGS method for large scale optimization. Mathematical programming 45:503-528. https://doi.org/10.1007/BF01589116
41. Cai Y, Zhang G, & Zhang YW (2014) Polarity-reversed robust carrier mobility in monolayer MoS_2 Journal of the American Chemical Society 136:6269-6275. https://doi.org/10.1021/ja4109787

42. Yun WS, Han SW, Hong SC, Kim IG, & Lee JD (2012) Thickness and strain effects on electronic structures of transition metal dichalcogenides: 2H-M X 2 semiconductors (M= Mo, W; X= S, Se, Te). Physical Review B 85:033305. https://doi.org/10.1103/PhysRevB.85.033305
43. Yue Q, Kang J, Shao Z, Zhang X, Chang S, Wang G, Qin S & Li, J (2012) Mechanical and electronic properties of monolayer MoS2 under elastic strain. Physics Letters A 376:1166-1170. https://doi.org/10.1016/j.physleta.2012.02.029
44. Sengupta A, Ghosh RK, & Mahapatra S (2013) Performance Analysis of Strained Monolayer MoS_2 IEEE transactions on electron devices, 60:2782-2787. https://doi.org/10.1109/TED.2013.2273456

Figures

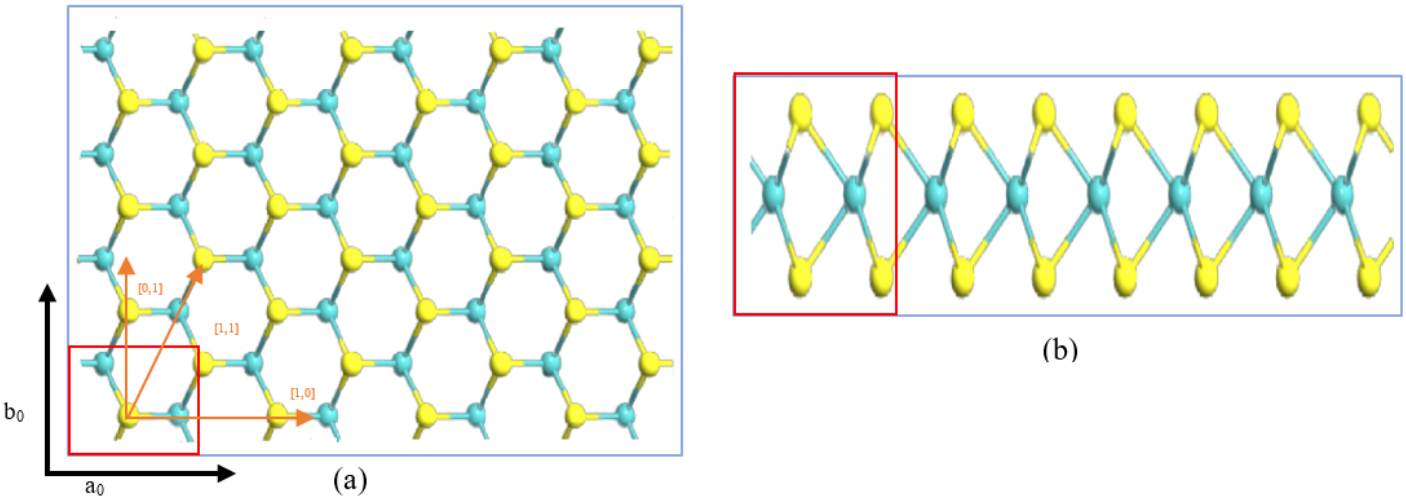

Figure 1

The atomic structure of MoS2 monolayer (a) Top view and (b) Side view

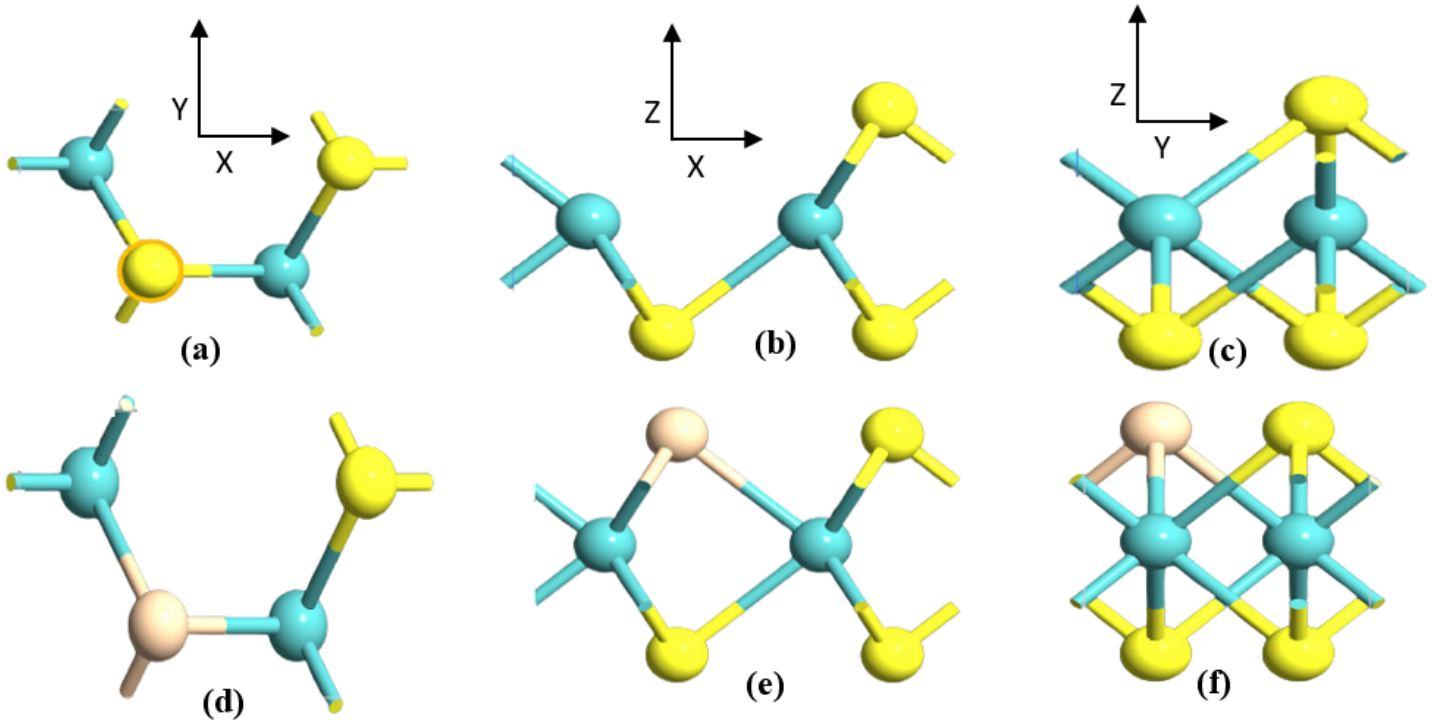

Figure 2

(a, b, c) Structure of defected and (d, e, f) Si-doped MoS2 monolayer

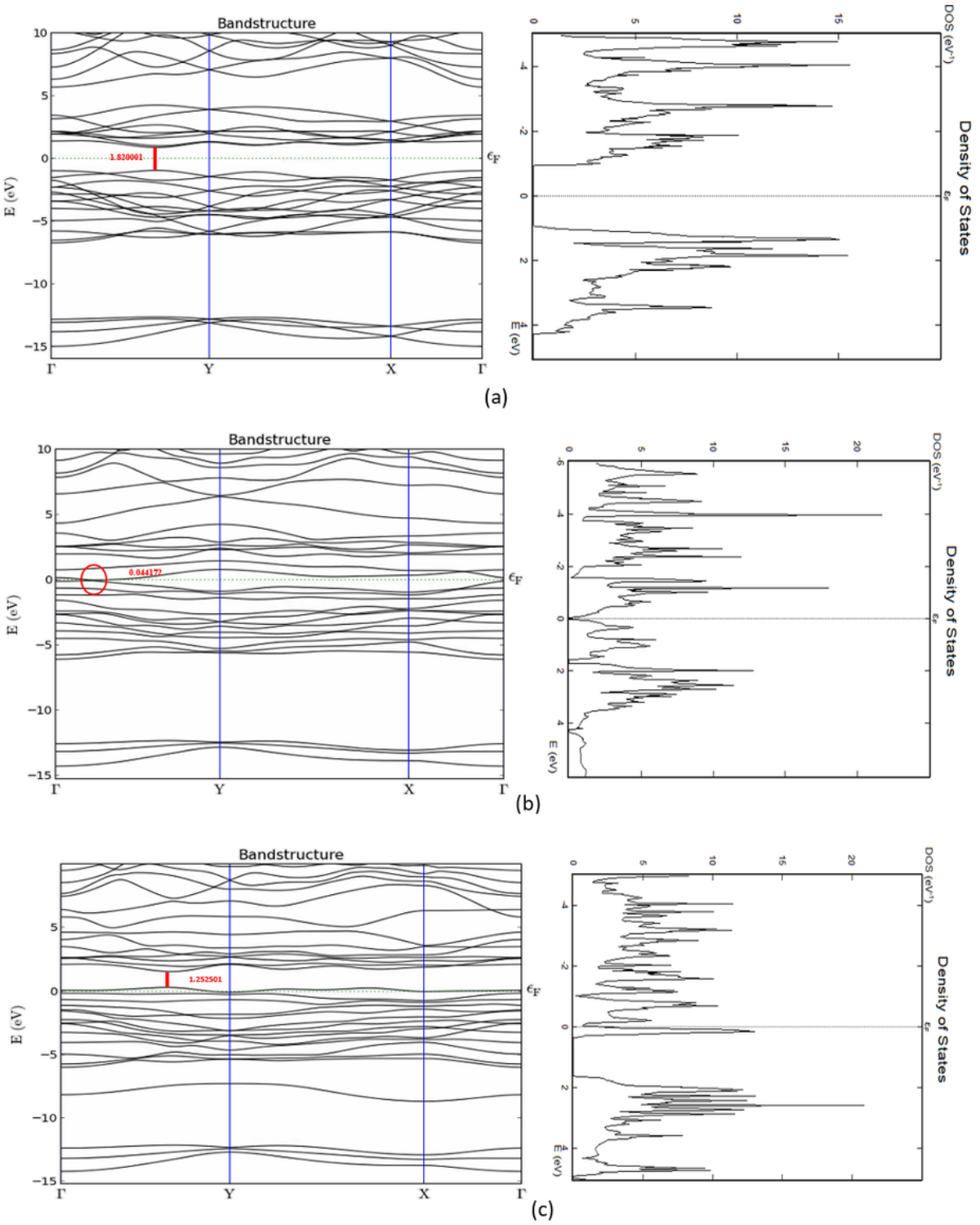

Figure 3

Band structure along with density of states (DoS) for (a) MoS2 monolayer (b) defected MoS2 monolayer (c) Si-doped MoS2 monolayer without strain

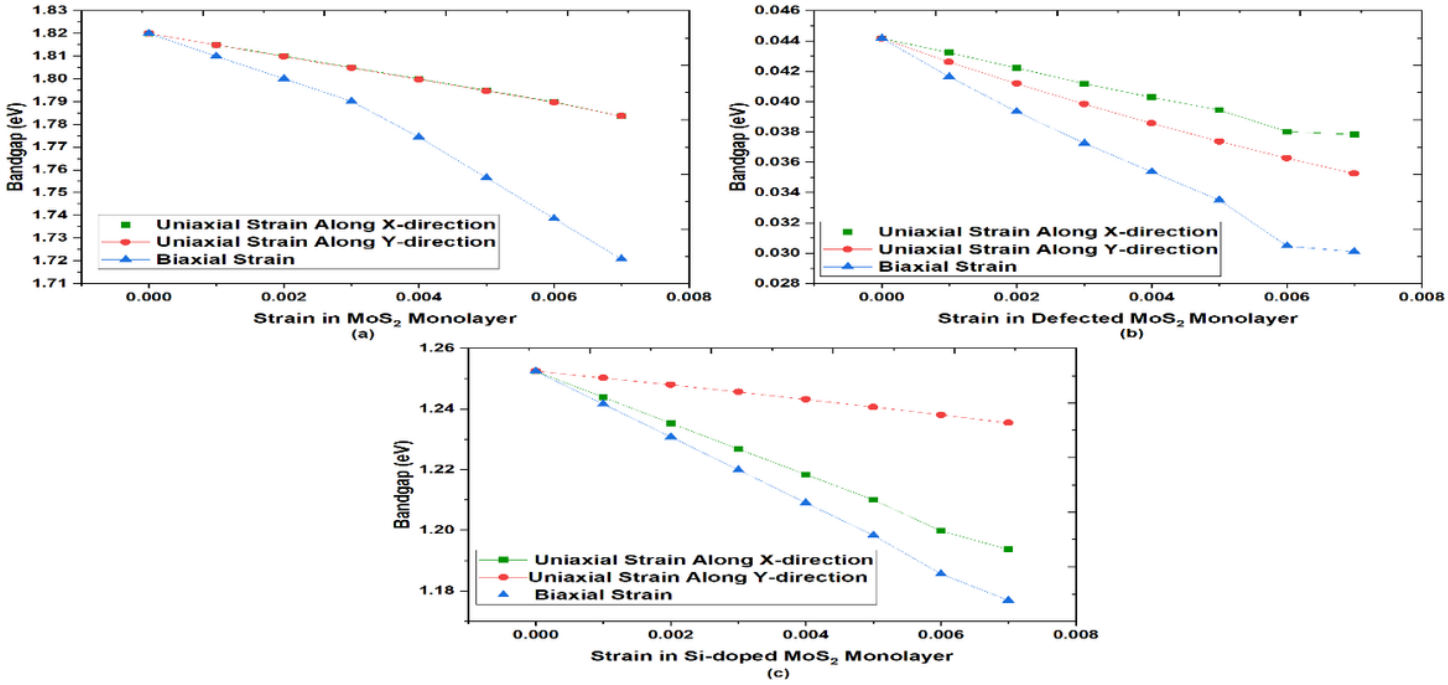

Figure 4

Band structure as a function MoS2 structure with strain along different directions.

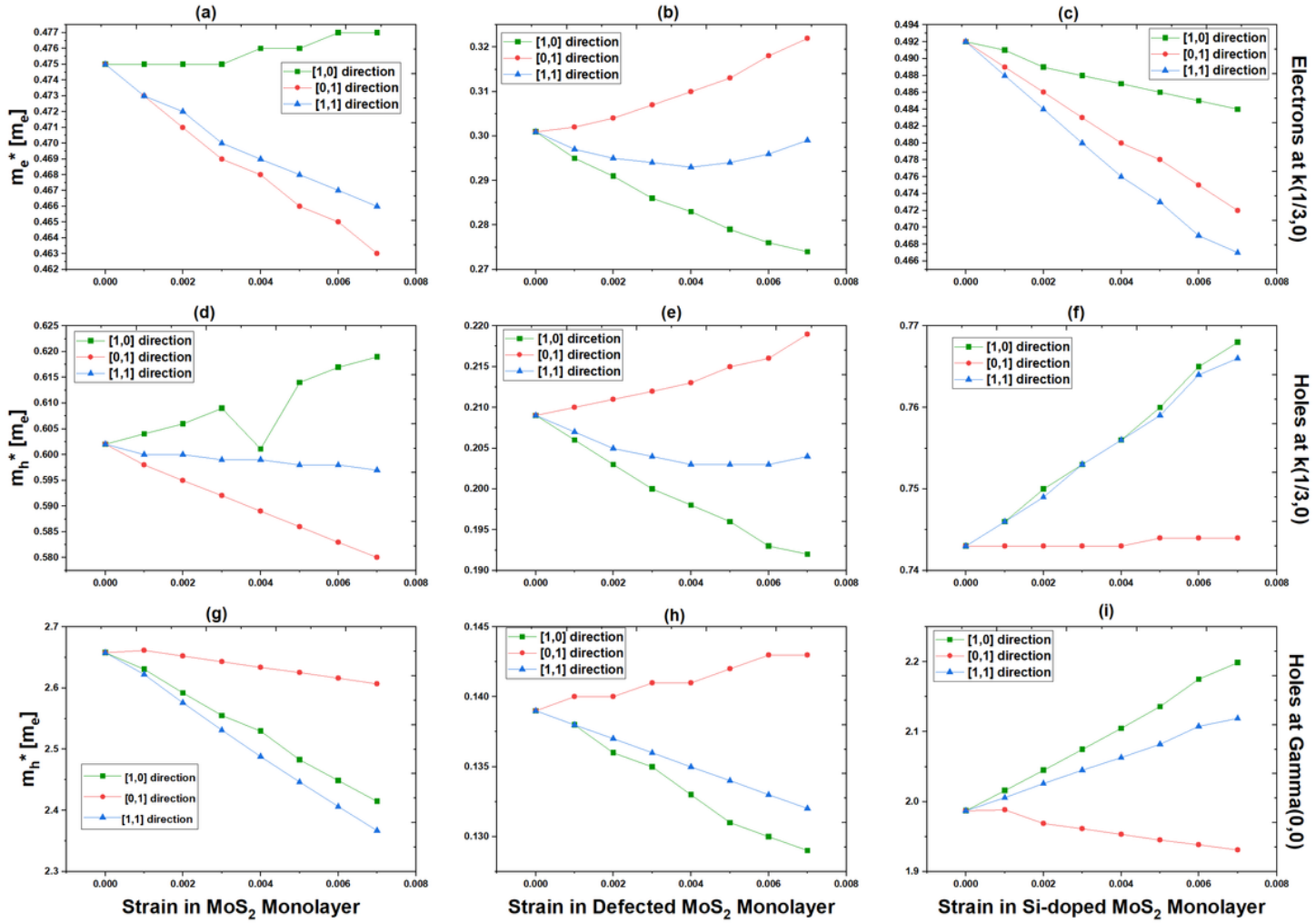

Figure 5

The effective mass for electron and holes at fractional K-points and at Γ-points for different structures of MoS2 monolayer under tensile strain along [1,0], [0,1] and [1,1] directions of monolayer.

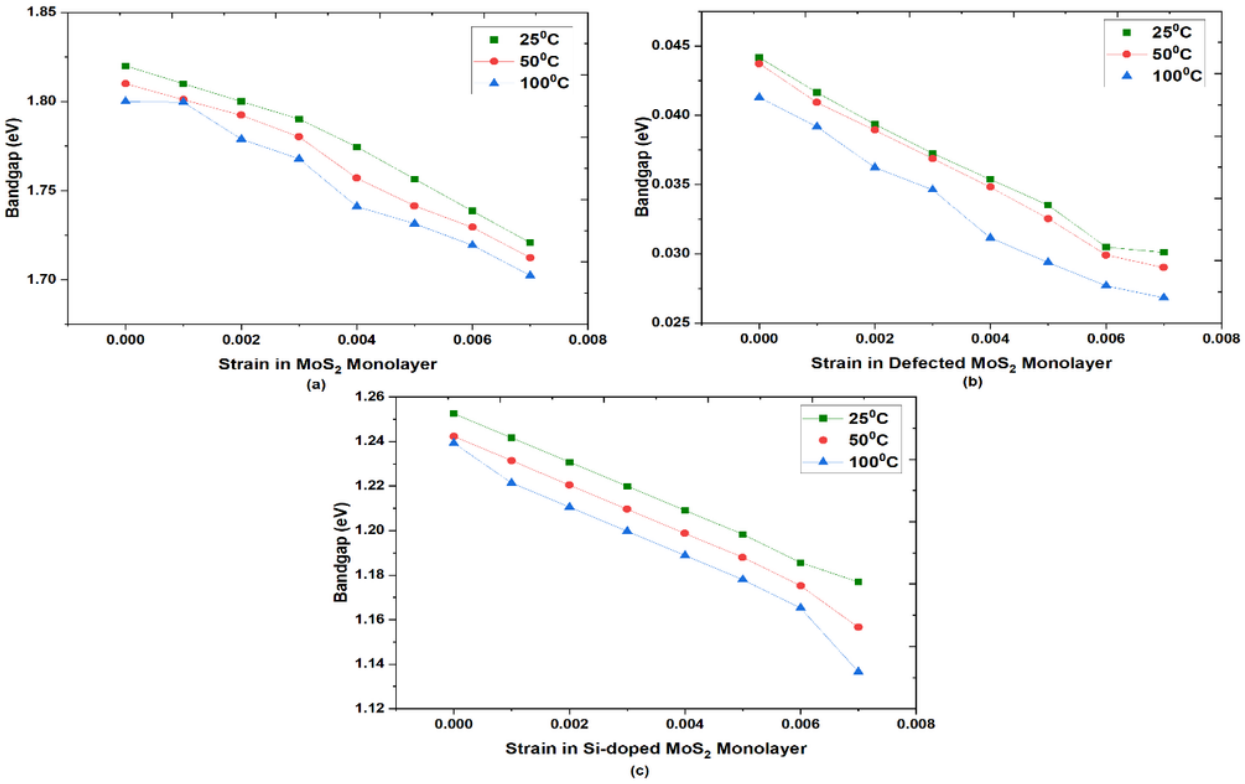

Figure 6

Temperature variation in bandgap with respect to biaxial tensile strain